Physics and Chemistry of Minerals (2022) 49:46
https://doi.org/10.1007/s00269-022-01222-5

ORIGINAL PAPER

# High-pressure behavior of gasparite-(Ce) (nominally $CeAsO_4$), a monazite-type arsenate

Francesco Pagliaro[1] · Paolo Lotti[1] · Davide Comboni[2] · Tommaso Battiston[1] · Alessandro Guastoni[3] · Patrizia Fumagalli[1] · Nicola Rotiroti[1] · G. Diego Gatta[1]

Received: 11 August 2022 / Accepted: 19 October 2022


## Abstract

The high-pressure behavior of the natural arsenate gasparite-(Ce) [$Ce_{0.43}La_{0.24}Nd_{0.15}Ca_{0.11}Pr_{0.04}Sm_{0.02}Gd_{0.01}(As_{0.99}Si_{0.03}O_4)$] from the Mt. Cervandone mineral deposit (Piedmont Lepontine Alps, Italy), has been studied by in situ single-crystal synchrotron X-ray diffraction up to 22.01 GPa. Two distinct high-pressure ramps have been performed, using a 16:3:1 methanol:ethanol:water solution and helium as *P*-transmitting fluids, respectively. No phase transition occurs within the pressure range investigated, whereas a change in the compressional behavior has been observed at ~ 15 GPa. A second-order Birch-Murnaghan EoS was fitted to the *P*-*V* data, leading to a refined bulk modulus of 109.4(3) GPa. The structural analysis has been carried out on the basis of the refined structure models, allowing the description of the deformation mechanisms accommodating the bulk compression in gasparite-(Ce) at the atomic scale, which is mainly controlled by the compression of the Rare Earth Elements coordination polyhedra, while the $AsO_4$ tetrahedra behave as a quasi-rigid units. A micro-Raman spectroscopy analysis, performed at ambient conditions, suggests the presence of hydroxyl groups into the structure of the investigated gasparite-(Ce).

**Keywords** Gasparite-(Ce) · Rare earth elements · Arsenate · Monazite · Synchrotron · High-pressure

## Introduction

The $ATO_4$ compounds (where $A$ = Sc, Y, La-Lu series (Ln), Ca, U and Th, whereas $T$ stands for tetrahedrally-coordinated cations) represent a large group of minerals. The $ATO_4$ group embodies several Rare Earth Elements (REE) bearing phosphates, arsenates and vanadates, in addition to, among the others, silicates, chromates and selenates. The $REETO_4$ phosphates, arsenates and vanadates can crystalize in both a zircon-type structure (also called xenotime-type) and in a monazite-type structure (Clavier et al. 2011). The zircon-type-structure is characterized by a tetragonal unit-cell (space group $I4_1/amd$; $Z$=4) and, in general, hosts the smaller Heavy Rare Earth Elements (HREE; Tb-Lu and Y, according to the classification provided by the U.S. Geological Survey, 2011) or Sc. Conversely, the monazite-type-structure REE-bearing minerals, with a monoclinic lattice (space group $P2_1/n$) ($Z$ = 4), typically host Light Rare Earth Elements (LREE; Ce-Gd, *i.e.*, the lanthanides with unpaired 4*f* electrons, according to U.S. Geological Survey, 2011). The first description of the monazite-type structure has been reported by Mooney (1948), who investigated the La, Ce, Pr and Nd phosphates. The structure has been later described correctly by Beall et al. (1981), Mullica et al. (1984) and Ni et al. (1995), whereas an exhaustive review of the monazite-structure topology has been carried out by Boatner (2002) and then by Clavier et al. (2011). The monazite-type structure is characterized by infinite chains running along the [001] direction ($c$ axis), composed by the alternation of the $A$-coordination polyhedra (hereafter REE-coordination polyhedra) and the $T$-hosting tetrahedra (Fig. 1). The REE-polyhedron coordination environment is made by nine oxygen atoms. According to Mullica et al. (1984), the $REEO_9$ polyhedron can be described as an equatorial pentagon (sharing vertices with five $TO_4$ tetrahedra of five adjacent chains),

✉ Francesco Pagliaro
francesco.pagliaro@unimi.it

[1] Dipartimento di Scienze della Terra, Università degli Studi di Milano, Via Botticelli 23, 20133 Milan, Italy

[2] European Synchrotron Radiation Facility, 71 Avenue Des Martyrs, CS40220, 38043 Grenoble Cedex, France

[3] Dipartimento di Geoscienze, Università degli Studi di Padova, Via Gradenigo, 6, 35137 Padua, Italy

Published online: 15 November 2022

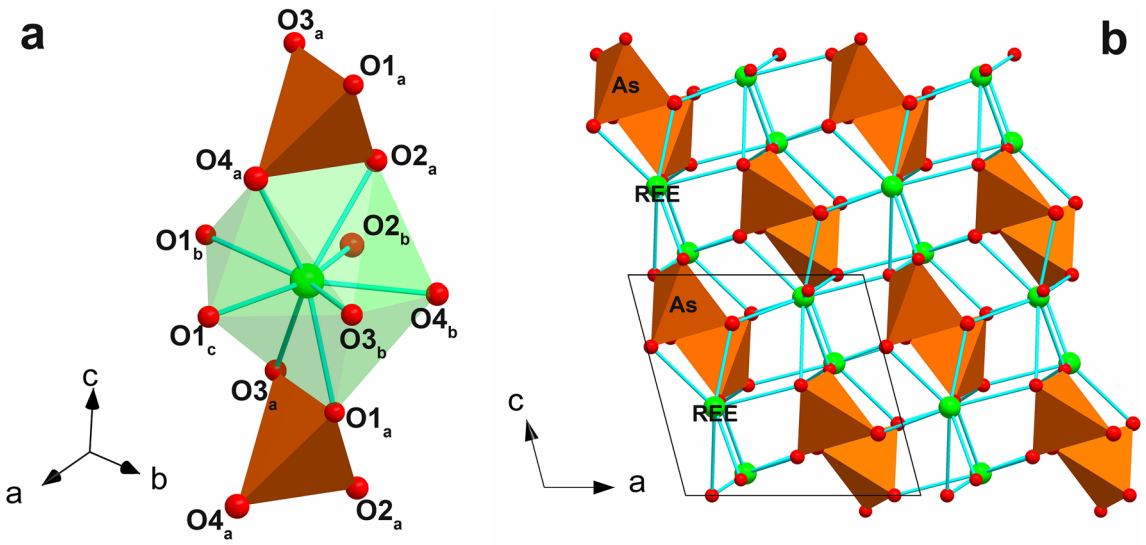


**Fig. 1** Fragment of the crystal structure of gasparite-(Ce), showing the nine REE-O bond distances, the REE atom in green, the As-tetrahedron in orange and the oxygen atoms in red (**a**); a general view down the [010] direction (**b**)

interpenetrated by a tetrahedron (made by the $O1_a$, $O2_a$, $O3_a$ and $O4_a$ oxygen atoms, see Fig. 1a), which is in contact, along the [001] direction, with two subsequent $TO_4$ tetrahedra, leading to the formation of the infinite chain units. As reported in Fig. 1a, the REE-$O2_a$ bond length is sharply longer than the other REE-O bonds, contributing to a significant distortion of the $REEO_9$ polyhedron (Clavier et al. 2011; Ni et al. 1995; Beall et al. 1981). Whether the monazite or the zircon structure is stable at ambient conditions strongly depends on the ionic radii of either oxygen, *A*- and *T*-site cations. This relation has been enlightened by Muller and Roy (1974), Fukunaga and Yamaoka (1979) and Bastide (1987). Pure $REEAsO_4$ compounds have been synthesized by Glushko et al. (1972), who observed the presence of both the monazite- and zircon-type structure topologies as a function of the radii of the REE-atoms. Whether the REE is one of the larger REE-cations, as La, Ce, Pr, and Nd, the lattice is monoclinic, whereas when REE = Y, Sc, Sm, Eu, Gd, Tb, Dy, Ho, Er, Tm, Yb, Lu the tetragonal zircon-type structure occurs in arsenates (Glushko et al. 1972; Ushakov et al. 2001; Boatner, 2002; Kolitsch and Holtstam, 2004). Chernovite-(Y) and gasparite-(Ce) are the natural arsenates with zircon- and monazite-type structure, respectively, and they are both rare minerals. As underlined by Vereshchagin et al. (2019), gasparite-(Ce), similarly to the Y- and HREE-bearing arsenate chernovite-(Y), seems strongly linked to post-magmatic and metasedimentary environments, influenced by late hydrothermal processes. The monazite-type structure in REE-bearing arsenates had been firstly described from synthetic $CeAsO_4$ by Beall et al. (1981) and only after Graeser and Schwander (1987) it has been reported in nature, in the mineral named gasparite-(Ce), occurring within the hydrothermal Alpine fissures of Mt. Cervandone (Italy) and adjacent Binn Valley (Switzerland). For a complete overview about the sites where gasparite-(Ce) occurs, refer to Ondrejka et al. (2007), Anthony et al. (2000), Kolitsch et al. (2004), Mills et al. (2010), Mancini (2000), Vereshchagin et al. (2019), Cabella et al. (1999).

The high-pressure behavior of monazite-type phosphates has been object of numerous studies (Lacomba-Perales et al. 2010; Errandonea et al. 2018; Errandonea 2017; Feng et al. 2013; Ruiz-Fuertes et al. 2016; Heffernan et al. 2016; Huang et al. 2010; Li et al. 2009), while the literature available on arsenates is rather limited (Metzger et al. 2016; Li et al. 2009). A comprehensive theoretical study on the high-pressure behavior of all the REE-bearing arsenates and phosphates, with both zircon- and monazite-type structure, has been reported by Li et al. (2009), whereas an extensive review on the high-pressure behavior of monazite-type $ATO_4$ compounds has been carried out by Errandonea (2017). Generally, what has been observed in synthetic REE-phosphates end members (Lacomba-Perales et al. 2010; Feng et al. 2013; Li et al. 2009; Errandonea 2017) is that the bulk modulus increases (*i.e.*, the compressibility decreases) when the atomic radius of the REE cation decreases, from $LaPO_4$ to $GdPO_4$. In the same way, the pressure stability field of the monazite-structured phosphates increases to higher pressures from $LaPO_4$ to $GdPO_4$. For $LaPO_4$, a phase transition at a pressure exceeding 27.1 GPa to a post-barite-type structure ($P2_12_12_1$ space group) occurs and the same phase transition is predicted to occur at 35 and 45 GPa for $NdPO_4$ and $GdPO_4$, respectively (Lacomba-Perales et al. 2010; Ruiz-Fuertes et al. 2016; Errandonea 2017). Whereas several

studies have been dedicated to the compressional behavior of the monazite-structure analogs, a few of them explore the structural mechanisms responsible for the high-pressure bulk compression and deformation. Heffernan et al. (2016) studied the structural (at the atomic scale) response of $GdPO_4$ under high-pressure conditions up to 7.062 GPa. Either Heffernan et al. (2016), Errandonea et al. (2018) and Muñoz and Rodríguez-Hernández (2018) point out the relevant role played by the compression of the $REEO_9$ polyhedron, whereas the $PO_4$ tetrahedra substantially act as rigid bodies. Heffernan et al. (2016) also show that the anisotropic behavior of $GdPO_4$ is mainly controlled by the variations of the O−Gd−P linkages, resulting from the distortion of the $GdO_9$ polyhedra. So far, no experimental high-pressure study has been performed on REE-arsenates with the monazite structure, neither synthetic nor natural, with the exception of the study of Metzger et al. (2016) on the monazite-to-scheelite phase transition in LREE arsenates.

In this study, we have investigated the high-pressure behavior of a natural gasparite-(Ce), with a multi-elemental composition of the REE-bearing *A* site, by means of in situ single-crystal synchrotron X-ray diffraction with a diamond anvil cell (DAC). The elastic parameters and a description of the deformation mechanisms accommodating and controlling, at the atomic scale, the bulk compression are provided, along with a comparative analysis of the high-*P* behaviors of gasparite-(Ce) and other monazite-type $ATO_4$ compounds. Moreover, the Raman spectrum of gasparite-(Ce) has been collected at ambient conditions, with the aim to provide a comprehensive chemical description of this mineral. This manuscript belongs to an ongoing long-term project studying the crystal chemistry and the behavior at non-ambient conditions of REE-bearing minerals (Gatta et al. 2019, 2021; Pagliaro et al. 2022).

## Materials and methods

Natural samples of hydrothermal gasparite-(Ce) from the Mt. Cervandone (Lepontine Alps, Italy) mineral deposit have been studied. Further information concerning the mineralogy of the REE-bearing deposit are reported by Dal Piaz (1975), Graeser and Roggiani (1976), Graeser and Albertini (1995), Guastoni et al. (2006), Demartin et al. (1991a, 1991b). The chemical composition of the samples of gasparite-(Ce) used in this study has been previously determined by electron probe microanalysis in wavelength dispersion mode (EPMA-WDS) based on eight points of analysis: $Ce_{0.43}La_{0.24}Nd_{0.15}Ca_{0.11}Pr_{0.04}Sm_{0.02}Gd_{0.01}(As_{0.99}Si_{0.03}O_4)$. Further information on the adopted experimental protocol is reported in Pagliaro et al. (2022).

### Raman spectroscopy

Unoriented micro-Raman spectroscopy analysis of gasparite-(Ce) has been carried out, at room conditions, at the Earth Science Department "A. Desio" of the University of Milano, using a Horiba LabRam HR Evolution micro-Raman spectrometer, equipped with an Nd-YAG 532 nm/100 mW, a Peltier-cooled charge-coupled device (CCD) detector, an Olympus microscope having 100 × objectives and Ultra Low Frequency (ULF) filters. In addition, the 10% laser power filter used yields to an esteemed power of 6 mW on the sample surface. The spectra were collected with the *Labspec* software in the region between 30 and 1200 $cm^{-1}$ and in the range 3200–4000 $cm^{-1}$, both with a step size of 1.8 $cm^{-1}$ and 20 s of acquisition time. The two sections of the micro-Raman spectrum of gasparite-(Ce) are reported in Fig. 2a and Fig. 2b. Peak analysis has been conducted using the *OriginPro* suite (OriginLab Corporation 2019).

### In situ high-pressure X-ray diffraction experiments

In situ high-pressure single-crystal synchrotron X-ray diffraction experiments have been conducted at the ID15b beamline of the European Synchrotron Radiation Facility, ESRF (Grenoble, France). Single crystals of gasparite-(Ce) (ca $20 \times 15 \times 10$ $\mu m^3$ in size) were selected for two separate high-pressure experiments, performed using a 16:3:1 methanol:ethanol:$H_2O$ mixture (hereafter *m.e.w.*, Angel et al. 2007), up to 9.31(5) GPa, and helium (Klotz et al. 2009), up to 22.76(5) GPa, as *P*-transmitting fluids, respectively. A convergent monochromatic X-ray beam with an energy of 30.2 keV ($\lambda = 0.41046$ Å) was used. For each *P*-point, the collection strategy consisted in a step-wise ω-scan in the range ± 30°, with a step-width of 0.5° and an exposure time of 0.5 s/frame (*m.e.w.* ramp) and 0.25 s/frame (He ramp). The pressure increase was controlled through a remote, automated pressure-driven system. X-ray diffraction patterns were collected with a MAR555 flat-panel detector, set at 260.32 mm from the sample position. The sample-to-detector distance was calibrated using a Si standard. Further details concerning the beamline setup are reported in Merlini and Hanfland (2013). For both the experiments, gasparite-(Ce) crystals were loaded in a membrane-driven diamond anvil cell (DAC), equipped with Boehler-Almax designed diamonds/seats with 60° opening and 600 μm culets size. Stainless-steel foils (with thickness ~ 250 μm) were pre-indented to ca. 70 μm and then drilled by spark-erosion to obtain *P*-chambers of 300 μm and 150 μm in diameter, for the *m.e.w.* and He ramps, respectively. Few ruby spheres were used as pressure calibrants (pressure uncertainty ± 0.05 GPa; Mao et al. 1986; Chervin et al. 2001). Indexing of the X-ray diffraction peaks, unit-cell refinements and intensity data reductions were performed using the *CrysAlisPro*

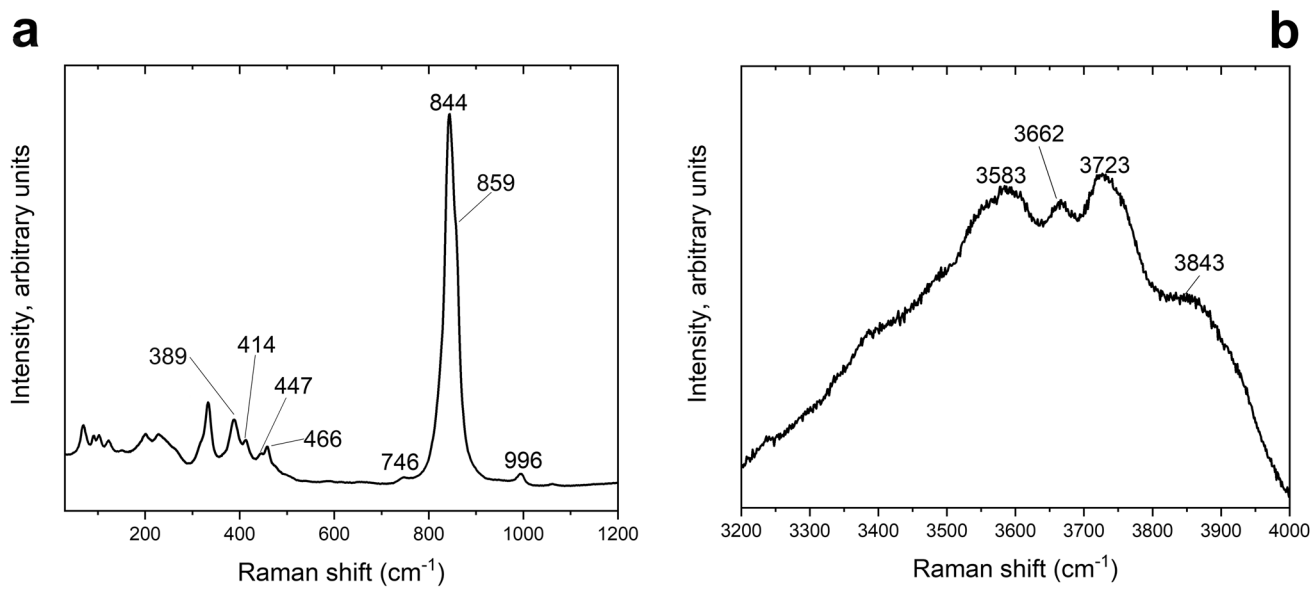


**Fig. 2** Raman spectra of gasparite-(Ce) in the range 30–1200 $cm^{-1}$ (**a**) and in the region (3200–4000 $cm^{-1}$) (**b**). See Table S2 for a complete list of the peaks and their assignments

package (Rigaku Oxford Diffraction 2019). Absorption effects, due to the DAC components, were corrected using the semi-empirical ABSPACK routine, implemented in *CrysAlisPro*.

### Structure refinements

The experimental X-ray diffraction patterns were always compatible with the monoclinic $P2_1/n$ symmetry of gasparite-(Ce). All the structure refinements were performed using the package *JANA2006* (Petříček et al. 2014), in the space group $P2_1/n$, using, as starting model, the atomic coordinates reported by Pagliaro et al. (2022). Only the structure refinements performed on the *m.e.w.*-ramp XRD data are fully reported (see High-pressure structure deformation for further details). The occupancies of all the crystallographic sites were fixed according to the measured chemical data, applying a cut-off on atomic species with abundance lower than 0.03 *atoms per formula unit* (apfu). Calcium was also excluded from the refinements, as this led to better figures of merit (further details on this protocol can be found in Pagliaro et al. 2022). For all the refinements based on in situ high-pressure diffraction data, to reduce the number of refined variables, the atomic displacement parameters (ADP) were refined as isotropic. At any *P* point, no restraints on bond distances or angles have been applied and all the refinements converged with no significant correlations among the refined variables. The refined structure models are deposited as supplementary materials (CIF files). Relevant statistical parameters of the refinements are reported in Table S1.

## Results and discussion

### Micro-Raman spectroscopy

Figure 2 shows the experimental micro-Raman spectra of gasparite-(Ce). Conversely to the previously studied monazite-type LREE-bearing arsenates (Vereshchagin et al. 2019; Botto and Baran 1982), gasparite-(Ce) from Mt. Cervandone, in the range between 3200 and 4000 $cm^{-1}$ (Fig. 2b), shows the presence of slightly intense peaks, ascribed to $OH^-$ groups. The partial replacement of oxygen atoms by hydroxyl groups may explain some features of the chemical data of gasparite-(Ce), characterized by a slight charge defect, for to the combined presence of $Ca^{2+}$ within the *A* site (in place of $REE^{3+}$) and $Si^{4+}$ within the tetrahedral *T*-site (in place of $As^{5+}$), apparently not counterbalanced (Pagliaro et al. 2022). As reported by Pagliaro et al. (2022), this may be explained by the following charge compensating mechanism:

$$2(OH)^- + Ca^{2+} + Si^{4+} = 2O^{2-} + REE^{3+} + (As)^{5+},$$

which is further supported by the present Raman spectrum of gasparite-(Ce).

Further information about the Raman spectroscopy data are reported as supplementary material (see Table S2).

### High-pressure behavior

#### Compressional behavior

Figure 3 and 4 and Table S3 show the compressional behavior of the unit-cell of gasparite-(Ce) up to 21.05 GPa.

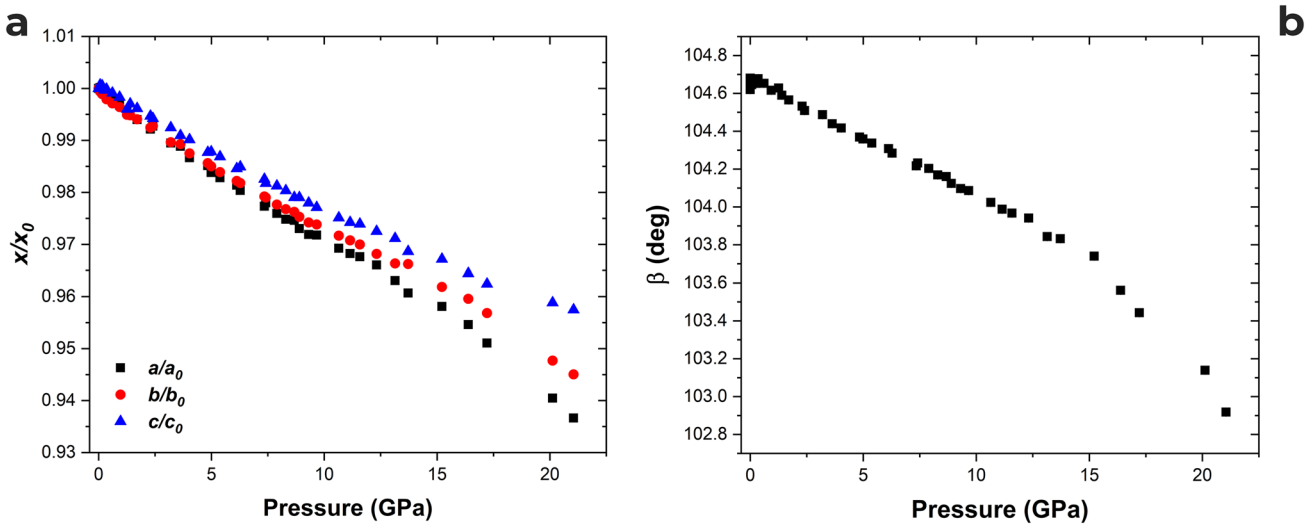


**Fig. 3** High-pressure evolution of unit-cell axial parameters (**a**) and of the $\beta$ angle of gasparite-(Ce) (**b**), showing the compressional change at ~ 15 GPa

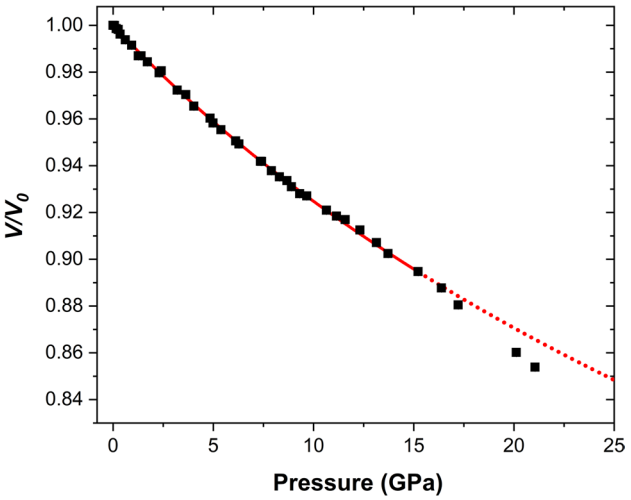


**Fig. 4** High-pressure evolution of the experimental unit-cell volume of gasparite-(Ce). The red line represents the fitted BM2-EoS, while the dotted red line line is an extension of the BM2-EoS at pressures exceeding the change in compressional behavior (see text for further details)

Gasparite-(Ce) is characterized by an anisotropic compressional behavior, with a lower compressibility along [001], a maximum shortening along [100], whereas along [010] displays an intermediate compressibility (Fig. 3a). At a first approximation, gasparite-(Ce) shows a similar compressional behavior with the other $ATO_4$ compounds sharing a monazite-type structure (Errandonea 2017). The monoclinic $\beta$ angle linearly decreases with pressure up to ~ 15 GPa, as shown in Fig. 3b. Although still linear, at pressures exceeding ~ 15 GPa, the monoclinic angle decreases more pronouncedly, reaching 102.91(1)° at 21.05 GPa (Fig. 3b). Above ~ 15 GPa an increase in the rate of unit-cell volume compression can also be observed. The compressional behavior of gasparite-(Ce) has been modeled with both a second-order Birch-Murnaghan Equation of State (BM2-EoS) and a third-order Birch-Murnaghan Equation of State (BM3-EoS) (Birch 1934; Angel 2000), using the *Eos_Fit7c_GUI* software (Angel et al. 2014; Gonzalez-Platas et al. 2016), based on both the *m.e.w.* and helium ramps unit-cell data (normalized to corresponding ambient-*P* values). The experimental data collected at pressures exceeding 15.22 GPa have not been taken into account, due to the observed change in the compressional behavior (Fig. 3b and Fig. 4). The fit of the BM-EoS to the experimental data yielded the following refined parameters: $K_{P0,T0} = 109.4(3)$ GPa ($\beta_V = 0.00914(3)$ GPa$^{-1}$) and $V_0 = 320.58(3)$ Å$^3$ for the BM2-EoS, $K_{P0,T0} = 108.3(10)$ GPa ($\beta_V = 0.00923(9)$ GPa$^{-1}$), $K' = 4.2(2)$ and $V_0 = 320.59(3)$ Å$^3$ for the BM3-EoS. An analysis of the finite Eulerian strain (*fe) vs.* the normalized pressure (*Fe*) plot [Figure S1; see Angel (2000) for further details] suggests that the refined BM2-EoS curve (reported in Fig. 4) properly describes the elastic compressional behavior of gasparite-(Ce). In addition, the compressional behaviors along the three principal crystallographic directions have been modeled with BM2-EoS. As for the *P–V* data, the fit of the BM2-EoS has been conducted on the normalized data up to 13.70 GPa, yielding the following results, where $K_{l0}$ is the refined linearized bulk modulus [see Angel (2000) for further details]: $K_{a0} = 93(4)$ GPa ($\beta_a = 0.00357(9)$ GPa$^{-1}$) and $a_0 = 6.9286(13)$ Å; $K_{b0} = 105(4)$ GPa ($\beta_b = 0.00318(9)$ GPa$^{-1}$) and $b_0 = 7.1265(9)$ Å; $K_{c0} = 122(4)$ GPa ($\beta_c = 0.00273(9)$ GPa$^{-1}$) and $c_0 = 6.7120(10)$ Å. Given the monoclinic symmetry of gasparite-(Ce), the

compressibility along the unit-cell axes does not allow a comprehensive description of the elastic anisotropy, due to the variation of the $\beta$ angle as a function of pressure. Therefore, magnitude and orientation of the finite Eulerian unit-strain tensor have been calculated based on the data from the helium ramp, between 0.0001 and 15.22 GPa, using the software *Win_Strain* (Angel 2011). The average compressibility values along the axes of the strain ellipsoid (with $\varepsilon_1 > \varepsilon_2 > \varepsilon_3$) are: $\varepsilon_1 = 0.00303(1)$ GPa$^{-1}$, $\varepsilon_2 = 0.002546(9)$ GPa$^{-1}$, $\varepsilon_3 = 0.001711(8)$ GPa$^{-1}$, leading to the following anisotropic scheme $\varepsilon_1$:$\varepsilon_2$:$\varepsilon_3 = 1.77$:$1.49$:$1$. The following matrix describes the geometric relations between the crystallographic axes and the strain ellipsoid orientation (where *X*//*a** and *Y*//*b*):

$$\begin{pmatrix} \varepsilon_1 \\ \varepsilon_2 \\ \varepsilon_3 \end{pmatrix} \measuredangle \begin{pmatrix} 23.7(2)^\circ & 90^\circ & 127.4(2)^\circ \\ 90^\circ & 180^\circ & 90^\circ \\ 113.7(2)^\circ & 90^\circ & 142.6(2)^\circ \end{pmatrix} \bullet \begin{pmatrix} a \\ b \\ c \end{pmatrix}$$

The matrix shows that both the directions of maximum and minimum compressibility lay on the (010) plane.

As previously mentioned, the monazite-type structure of gasparite-(Ce) undergoes a change in the compressional behavior, pointed out by the significant deviation in the $\beta$,*V vs. P* trends at $P > 15.22$ GPa. It is worth to underline that a similar behavior of the $\beta$,*V vs. P* trends was also described by Huang et al. (2010) for the synthetic powder samples of $CePO_4$ at about 11.5 GPa, compressed in methanol-ethanol (4:1) mixture. A careful analysis of the systematic absences in the experimental single-crystal diffraction patterns of this study suggests that no change in symmetry occurs coupled with the change in compressibility. In this case, as the experiment was conducted using a single crystal compressed in helium, we can exclude that the observed change in the compressional behavior may be ascribed to non-hydrostatic conditions. The structural mechanism likely responsible for this change in the elastic behavior is discussed in the next High-pressure structure deformation Section.

As discussed in Introduction Section, no experimental data about the elastic properties of the monazite-type arsenates have ever been experimentally obtained. The bulk modulus of gasparite-(Ce) ($K_{V0} = 109.4$ GPa) is lower than the theoretical bulk moduli determined by Li et al. (2009) for both $LaAsO_4$ and $CeAsO_4$ ($K_{V0} = 124.5$ GPa and $K_{V0} = 125.1$ GPa, respectively). On the other hand, it is worth to mention that also the theoretical bulk moduli obtained by Li et al. (2009) for monazite-type phosphates usually overestimate the experimental ones. Moreover, since different bulk moduli have been refined or calculated for $CePO_4$, ranging from 109(1) to 122 GPa (Errandonea et al. 2017; 2018; Huang et al. 2010), it is not straightforward to provide a comparison between gasparite-(Ce) and the large family of synthetic monazite-type $REEPO_4$, also in the light of the multi-elemental composition of the *A* site of the investigated natural sample. Considering the most recent and complete data, provided by Errandonea et al. (2018) on $CePO_4$ ($K_{V0} = 117.3(5)$ GPa, $K' = 4.54(3)$ refined with a BM3-EoS), the high-pressure compressibility of gasparite-(Ce) is slightly higher. This difference could be ascribed to the complex composition of the REE-bearing site in gasparite-(Ce) or to the presence of arsenic in place of phosphorous at the tetrahedral site, or by a combination of the two factors. Several authors (Li et al. 2009; Errandonea et al. 2011a; b) pointed out that, at a given composition of the REE cation, the arsenates are always more compressible than the phosphates counterparts, due to the higher compressibility of the $AsO_4$ with respect to the $PO_4$ tetrahedron. In addition, as pointed out by Pagliaro et al. (2022), the *T*-site of arsenates and phosphates has a strong influence on the whole structural features and, in particular, on the volume of both the REE-coordination polyhedron and unit-cell. Thus, the REE polyhedron in monazite-(Ce) is smaller, if compared to the REE polyhedron in gasparite-(Ce), despite a very similar population of the REE site. In this light, being the $PO_4$ tetrahedra less compressible than the $AsO_4$ ones, the smaller REE polyhedron of phosphates is reasonably also less compressible than the larger REE polyhedron of arsenates.

Interestingly, the bulk modulus of gasparite-(Ce) is intermediate between those of synthetic $REEPO_4$ and $LaVO_4$ ($K_{V0} = 95(5)$ GPa; Errandonea et al. 2016): the volume of $AsO_4$ is, indeed, intermediate between those of the $PO_4$ and $VO_4$ tetrahedra ($LaVO_4$ is the only endmember vanadate crystallizing with the monazite-type structure, if synthesized under high-temperature conditions, according to Bashir and Khan (2006), Rice and Robinson (1976), Aldred (1984), Baran and Aymonino (1971)).

## High-pressure structure deformation

The analysis of the structural deformation mechanisms, acting at the atomic scale, is mainly based on the experimental data from the *m.e.w.* ramp. Indeed, most of the analysis of the refined structural models from the He ramp revealed a scattering of the *P*-induced evolution of relevant structural parameters. Figure 5 and Table S4 show the high-pressure volume evolution for both the $REEO_9$ and the $AsO_4$ coordination polyhedra. The volumes of the coordination polyhedra have been measured by means of the routine implemented in the *Vesta 3* software (Momma and Izumi 2011).

A second-order Birch-Murnaghan EoS ($K' = 4$) fitted to the *P*–*V* data of the $REEO_9$ polyhedron leads to a refined bulk modulus of $K_{P0,T0} = 99(3)$ GPa ($\beta_V = 0.0101(9)$ GPa$^{-1}$; $V_0 = 33.02(4)$ Å$^3$). The $AsO_4$ tetrahedron clearly shows a discontinuity in the compressional behavior, with a significant compression until 2.30 GPa, followed by a stiffening that makes this structural unit substantially uncompressible

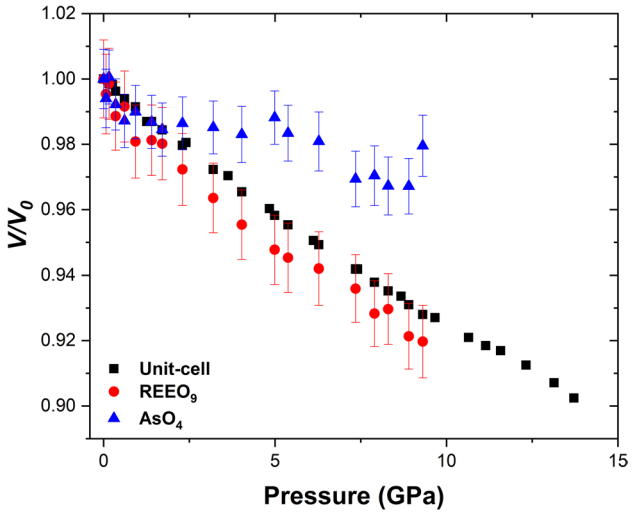


**Fig. 5** *P–V* diagram (normalized to ambient-conditions values) showing the compressional evolution of the unit-cell, $REEO_9$ and $AsO_4$ polyhedra volumes

between 2.30 and 9.31 GPa, preventing a modeling of its elastic behavior by an EoS. As the bulk compressibility of gasparite-(Ce) ($\beta_V = 0.00923(9)$ GPa$^{-1}$) is lower with respect to the compressibility of the $REEO_9$ coordination polyhedron ($\beta_{V\text{-REEO9}} = 0.0101(9)$ GPa$^{-1}$), it follows that the latter plays a key role in accommodating the unit-cell volume compression.

As reported in Fig. 6b and Table S5, the analysis of the high-pressure behavior of the REE-O bond distances shows that the $REEO_9$ polyhedron is characterized by a clear anisotropic behavior. The two REE-O bond distances involving the O3 atoms are the less compressible, with the REE-$O3_a$ bond distance even showing an expansion with the pressure increase. According to the notation reported in Fig. 1a, the REE-$O3_a$ bond distances, along with REE-$O2_a$ and REE-$O4_a$, represent the connection between the $REEO_9$ polyhedron and the $AsO_4$ tetrahedra along the *c* axis. The expansion of the REE-$O3_a$ bond distance, coupled with the contraction along the REE-$O1_a$ bond, leads to a tilting of the $AsO_4$ tetrahedra, with a slight closure of the REE-As-REE interatomic angle (Fig. 7d, Table S4). Therefore, we can conclude that the major mechanism responsible for the contraction along the *c* crystallographic direction is the bulk compression of the $REEO_9$ polyhedron, whereas a slight tilting of the $AsO_4$ polyhedron tends to accommodate this linear contraction.

In addition, the evolution with pressure of the REE-$O3_c$ interatomic distance, as it is defined in Fig. 8a, has been investigated. As shown in the normalized diagram in Fig. 8b, the REE-$O3_c$ interatomic distance is significantly more compressible compared to any other REE-O bond distance in the coordination sphere of the REE site and it shows a similar and rather significant compressional trend both in the *m.e.w.* and helium ramps. Between 13.72 and 17.22 GPa, the shortening of the REE-$O3_c$ undergoes a saturation before showing an abrupt compression above ~ 17 GPa, reaching the minimum value of 2.85(3) Å at 21.05 GPa. As the $O3_c$ oxygen (as defined in Fig. 8a) does not belong to the coordination sphere of the REE site at ambient conditions, we can conclude that, at *ca.* 15 GPa, the $REEO_9$ coordination polyhedron in gasparite-(Ce) experiences an increase in its coordination number from CN = 9 to CN = 10. This structural mechanism is likely responsible for the change in the compressional behavior shown in Fig. 3 and previously discussed.

Eventually, for a comprehensive understanding of the deformation mechanisms occurring in gasparite-(Ce) at high pressure, and to explain the anisotropic behavior described

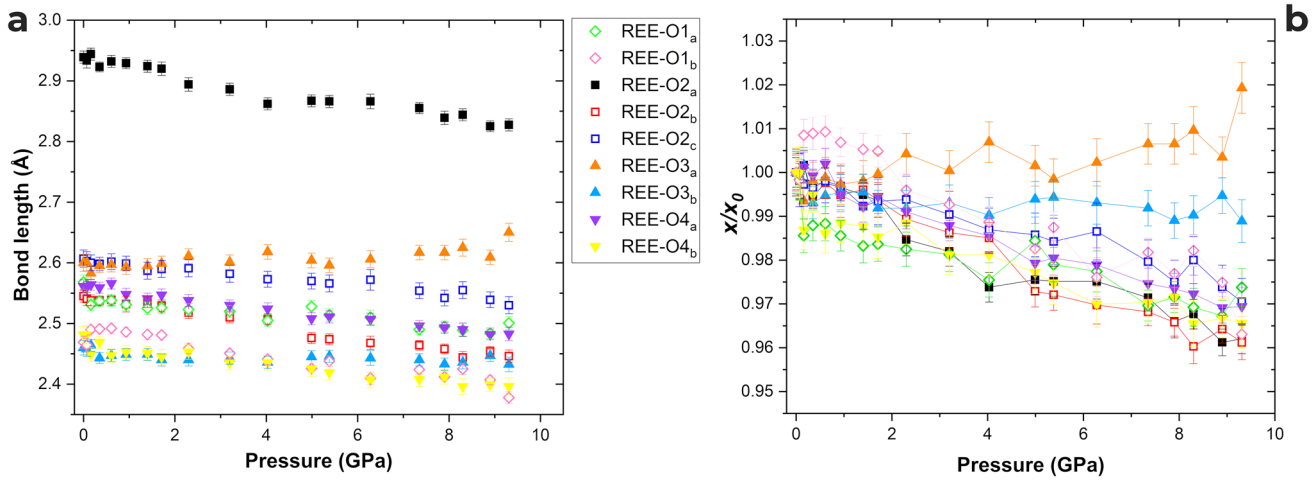


**Fig. 6** High-pressure evolution of the absolute (**a**) and normalized (to ambient conditions) values (**b**) of the nine independent REE-O bond distances

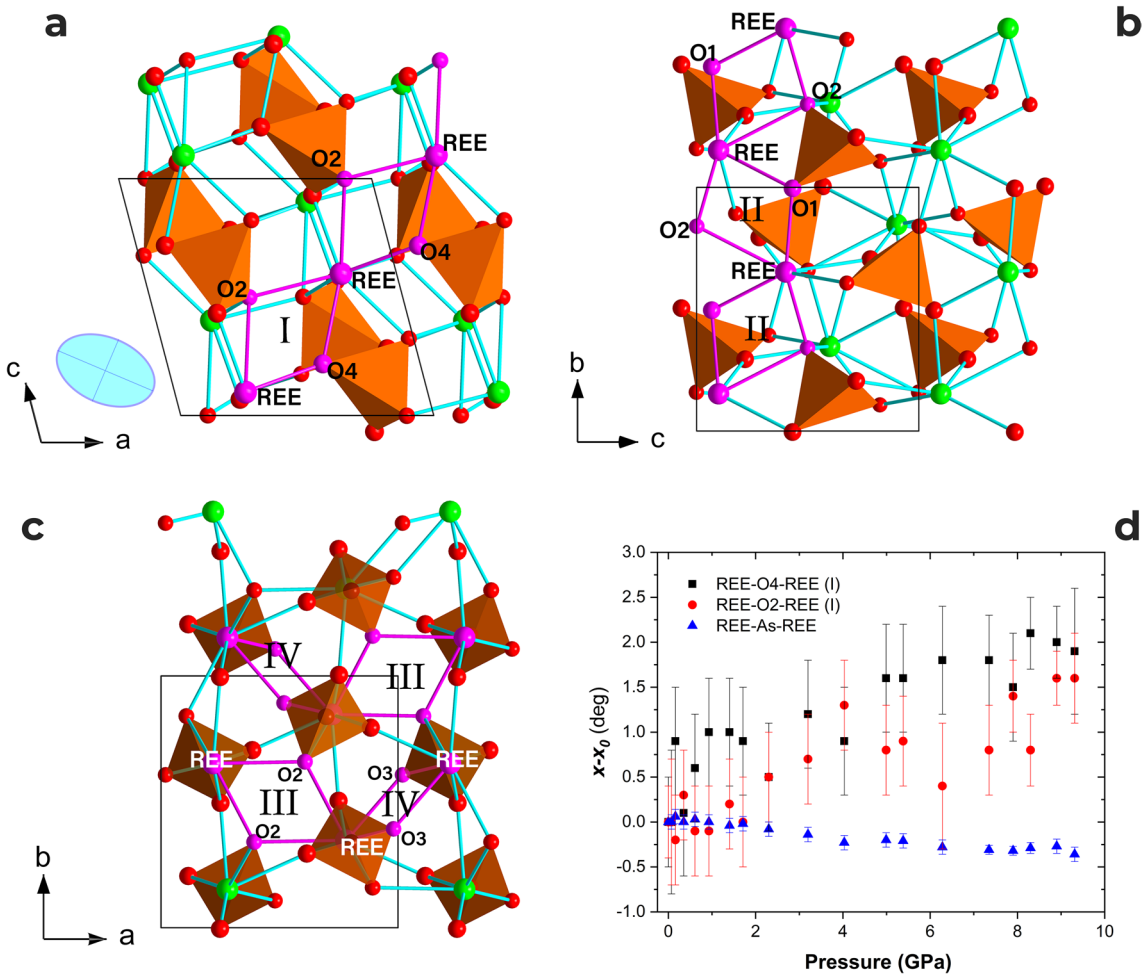


**Fig. 7** Representation of the crystal structure of gasparite-(Ce), showing the four independent lozenge-like units in purple (**a**, **b** and **c**) and high-pressure evolution of relevant interatomic angles (**d**); section of the Eulerian strain ellipsoid in the (010) plane (**a**)

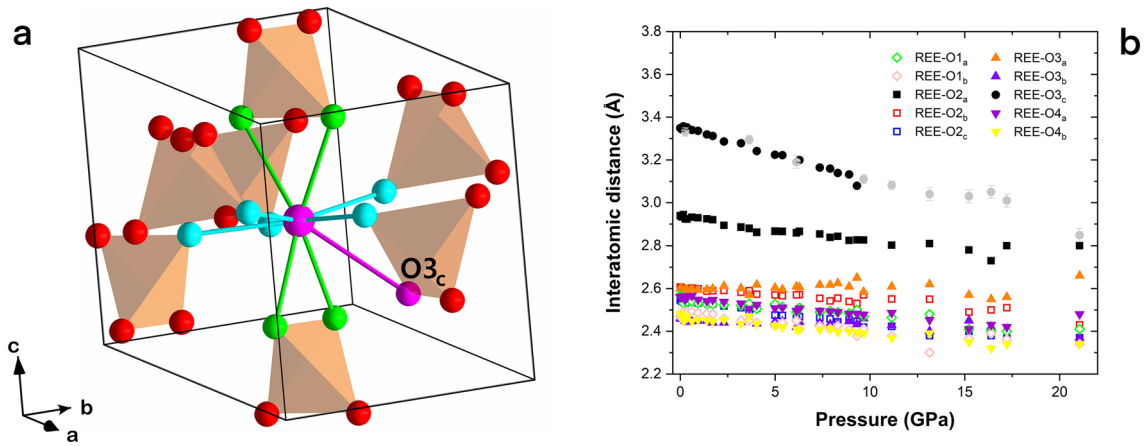


**Fig. 8** **a** Crystal structure of gasparite-(Ce) in the surrounding of the REE-bearing *A*-site: in purple is reported the longest REE-$O3_c$ interatomic distance, in sky blue the REE-O distances of the equatorial pentagon, while in green are reported the four REE-O chain-connecting bonds; **b** evolution with pressure of the ten REE-O interatomic distances (for the REE-$O3_c$ interatomic distance, the black and grey circles refer to the *m.e.w.* and He ramp respectively)

by the finite-strain tensor analysis, it is essential to introduce the REE-Ox-REE angles (Fig. 7a,b,c, Table S4), which represent the lozenge-like connection between adjacent chains. Six independent angular units, defining 4 independent lozenge-like connections (i.e., REE-O4-REE–REE-O2-REE (I); REE-O1-REE–REE-O2-REE (II), REE-O2-REE–REE-O2-REE (III); REE-O3-REE–REE-O3-REE (IV)) can be described as reported in Fig. 7a,b,c and Table S4. The only mechanism significantly contributing to the anisotropic compression involves the lozenge-like unit I, defined by the couple of interatomic angles REE-O2-REE and REE-O4-REE. These lozenge-like units define a slightly sinusoidal chain system running along the [101] direction, as reported in Fig. 7a. The opening of these two angles in response to the pressure increase, as shown in Fig. 7d, leads to a stretching of the chain. This deformation mechanism, coupled with the slight shortening of the REE-As-REE (Fig. 7d) chains running along the [001], provides the rationale for the anisotropic scheme defined by the finite-strain Eulerian tensor reported in Fig. 7a.

## Concluding remarks

The compressional behavior of the natural REE-bearing arsenate gasparite-(Ce) has been studied up to 21.05 GPa. The bulk compression of gasparite-(Ce) has been described with both a 2nd and 3rd order Birch-Murnaghan EoS up to 15.22 GPa, leading to a bulk modulus of $K_{P0,T0}=109.4(3)$ GPa ($V_0=320.58(3)$ Å$^3$, $K'=4$) and $K_{P0,T0}=108.3(10)$ GPa ($K'=4.23(20)$) and $V_0=320.59(3)$ Å$^3$), respectively. At pressure exceeding ~ 15 GPa, gasparite-(Ce) undergoes a change in the compressional behavior, clearly marked by a discontinuity in the compressional path of the $\beta$-angle (Fig. 3b), as previously also described for the isostructural synthetic $CePO_4$ (Huang et al. 2010). The analysis of the refined structure models suggests that this change of the compressional behavior is related to the increase in the coordination number of the *A*-site from 9 to 10 at $P>15$ GPa, with the $O3_c$ oxygen (Fig. 8) entering the coordination sphere of the REE cation in response to the *P*-induced structure deformation. The structural refinements show that the compression of the $REEO_9$ coordination polyhedron ($K_{P0,T0}=99(3)$ GPa; $V_0=33.02(4)$ Å$^3$) mostly accommodates the bulk compression of gasparite-(Ce), whereas the $AsO_4$ units behave as almost rigid bodies at *P* exceeding 2.30 GPa. Moreover, the structural analysis also showed that a modest tilting occurs within the [001] chain units, represented by the evolution of REE-As-REE interatomic angle (Fig. 7). Finally, the high-pressure evolution of six independent REE-O-REE bond angles, previously described (Fig. 7), has been taken into account to explain the anisotropy of the gasparite-(Ce) compressional behavior. It has been observed that the angular deformation of the couple made by the REE-O2-REE and REE-O4-REE angles is responsible for a stretching of the structure along the [101] direction, in agreement with the anisotropic scheme defined by the finite Eulerian strain tensor.

**Supplementary Information** The online version contains supplementary material available at https://doi.org/10.1007/s00269-022-01222-5.

**Acknowledgements** The editor, Larissa Dobrzhinetskaya, and two anonymous reviewers are gratefully thanked for the valuable comments that allowed a significant improvement of this manuscript. ESRF is acknowledged for the provision of beamtime. Enzo Sartori is gratefully thanked for providing the samples. FP, PL, TB, NR, PF and GDG acknowledge the Italian Ministry of University and Research (MUR) for the support through the project "*Dipartimenti di Eccellenza 2018-2022 – Le Geoscienze per la società: Risorse e loro evoluzione*" and the University of Milano for the support through the project "*Piano di sostegno alla Ricerca 2020*".

**Author contributions** FP, PL and GDG conceived and planned the experiments, AG and NR performed preliminary sample characterization, DC and TB carried out HP experiments, FP and PF carried out Raman experiments, FP analyzed experimental data, FP and PL wrote the orginal manuscript draft and all the authors contributed to final manuscript editing.

**Funding** Open access funding provided by Università degli Studi di Milano within the CRUI-CARE Agreement.

## Declarations

**Conflict of interest** The authors have no financial and competing interests to declare that are relevant to the content of this article.



## References

Aldred AT (1984) Cell volumes of $APO_4$, $AVO_4$, and $ANbO_4$ compounds, where A=Sc, Y, La–Lu. Acta Crystallogr B 40:569–574

Angel RJ (2000) Equations of state. In: Hazen RM, Downs RT (eds) High-temperature and high-pressure crystal chemistry: review in mineralogy and geochemistry, vol 41. Mineralogical Society of America and Geochemical Society, Washington, pp 35–59

Angel RJ (2011) Win_Strain. A program to calculate strain tensors from unit-cell parameters. http://www.rossangel.com/home.htm

Angel RJ, Bujak M, Zhao J, Gatta GD, Jacobsen SD (2007) Effective hydrostatic limits of pressure media for high-pressure crystallographic studies. J Appl Crystallogr 40:26–32

Angel RJ, Gonzalez-Platas J, Alvaro M (2014) EosFit7c and a fortran module (library) for equation of state calculations. Z Kristallogr 229:405–419

Anthony JW, Bideaux RA, Bladh KW, Nichols MC (2000) Handbook of mineralogy arsenates, phosphates, vanadates, vol IV. Mineral Data Publishing, Tucson

Baran EJ, Aymonino PJ (1971) Über Lanthanorthovanadat. Z Anorg Allg Chem 383:220–225

Bashir J, Khan MN (2006) X-ray powder diffraction analysis of crystal structure of lanthanum orthovanadate. Mater Lett 60:470–473

Bastide JP (1987) Systématique simplifiée des composés $ABX_4$ ($X=O^{2-}$, $F^-$) et evolution possible de leurs structures cristallines sous pression. J Solid State Chem 71:115–120

Beall GW, Boatner LA, Mullica DF, Milligan WO (1981) The structure of cerium orthophosphate, a synthetic analogue of monazite. J Inorg Nucl 43:101–105

Boatner LA (2002) Synthesis, structure, and properties of monazite, pretulite, and xenotime. Rev Mineral Geochem 48:87–121

Botto IL, Baran EJ (1982) Characterization of the monoclinic rare earth orthoarsenates. J Less-Common Mat 83:255–261

Cabella R, Lucchetti G, Marescotti P (1999) Occurrence of LREE- and Y-arsenates from a Fe-Mn deposit, Ligurian Brianconnais Domain, Maritime Alps, Italy. Canad Mineral 37:961–972

Chervin JC, Canny B, Mancinelli M (2001) Ruby-spheres as pressure gauge for optically transparent high pressure cells. High Press Res 21:305–314

Clavier N, Podor R, Dacheux N (2011) Crystal chemistry of the monazite structure. J Eur Ceram Soc 31:941–976

Dal Piaz G (1975) La val Devero ed i suoi minerali. Memorie Istituto Geologia Università di Padova, Volume X. Società Cooperativa Tipografica, Padova

Demartin F, Pilati T, Diella V, Donzelli S, Gentile P, Gramaccioli CM (1991a) The chemical composition of xenotime form fissures and pegmatites in the Alps. Canad Mineral 29:69–75

Demartin F, Pilati T, Diella V, Donzelli S, Gramaccioli CM (1991b) Alpine monazite; further data. Canad Mineral 29:61–67

Errandonea D (2017) High-pressure phase transitions and properties of $MTO_4$ compounds with the monazite-type structure. Phys Status Solidi B 254:1700016

Errandonea D, Kumar R, Lopez-Solano J, Rodriguez-Hernandez P, Muñoz A, Rabie MG, Puche RS (2011a) Experimental and theoretical study of structural properties and phase transitions in $YAsO_4$ and $YCrO_4$. Phys Rev B 83:134109

Errandonea D, Kumar RS, Achary SN, Tyagi AK (2011b) In situ high-pressure synchrotron x-ray diffraction study of $CeVO_4$ and $TbVO_4$ up to 50 GPa. Phys Rev B 84:224121

Errandonea D, Pellicer-Porres J, Martinez-Garcia D, Ruiz-Fuertes J, Friedrich A, Morgenroth W, Popescu C, Rodríguez-Hernandez P, Muñoz A, Bettinelli M (2016) Phase stability of lanthanum orthovanadate at high pressure. J Phys Chem C 120:13749–13762

Errandonea D, Gomis O, Rodríguez-Hernández P, Muñoz A, Ruiz-Fuertes J, Gupta M, Achary SN, Hirsch A, Manjon FJ, Peters L, Roth G, Tyagi AK, Bettinelli M (2018) High-pressure structural and vibrational properties of monazite-type $BiPO_4$, $LaPO_4$, $CePO_4$, and $PrPO_4$. J Condens Matter Phys 30:065401

Feng J, Xiao B, Zhou R, Pan W (2013) Anisotropy in elasticity and thermal conductivity of monazite-type $REPO_4$ (RE= La, Ce, Nd, Sm, Eu and Gd) from first-principles calculations. Acta Mater 61:7364–7383

Fukunaga O, Yamaoka S (1979) Phase transformations in $ABO_4$ type compounds under high pressure. Phys Chem Min 5:167–177

Gatta GD, Milani S, Corti L, Comboni D, Lotti P, Merlini M, Liermann HP (2019) Allanite at high pressure: effect of REE on the elastic behaviour of epidote-group minerals. Phys Chem Miner 46:783–793

Gatta GD, Pagliaro F, Lotti P, Guastoni A, Cañadillas-Delgado L, Fabelo O, Gigli L (2021) Allanite at high temperature: effect of REE on the thermal behaviour of epidote-group minerals. Phys Chem Miner 48:1–16

Glushko V, Medvedev V, Bergman G, Vasilev BP, Gurvich LV, Alekseev VI, Kolesov VP, Yunga VS, Ioffe N, Vorabev AF, Reznitskii LA, Khodakovskii IL, Smirnova NL, Galchenko G, Baibuz VF (1972) Thermicheskie konstanti veshtestv. Academy of Science, Moscow, U.S.S.R.

Gonzalez-Platas J, Alvaro M, Nestola F, Angel R (2016) EosFit7-GUI: a new graphical user interface for equation of state calculations, analyses and teaching. J Appl Crystallogr 49:1377–1382

Graeser S, Roggiani AG (1976) Occurrence and genesis of rare arsenate and phosphate minerals around Pizzo Cervandone, Italy/Switzerland. Rend Soc Ital Mineral Petrog 32:279–288

Graeser S, Albertini C (1995) Wannigletscher Und Conca Cervandone. Lapis 20:52–56

Graeser S, Schwander H (1987) Gasparite-(Ce) and monazite-(Nd): two new minerals to the monazite group from the Alps. Schweiz Mineral Petro Mitt 67:103–113

Guastoni A, Pezzotta F, Vignola P (2006) Characterization and genetic inferences of arsenates, sulfates and vanadates of Fe, Cu, Pb, Zn from mount cervandone (Western Alps, Italy). Period Mineral 75:141–150

Heffernan KM, Ross NL, Spencer EC, Boatner LA (2016) The structural response of gadolinium phosphate to pressure. J Solid State Chem 241:180–186

Huang T, Lee JS, Kung J, Lin CM (2010) Study of monazite under high pressure. Solid State Commun 150:1845–1850

Klotz S, Chervin JC, Munsch P, Le Marchand G (2009) Hydrostatic limits of 11 pressure transmitting media. J Phys D Appl Phys 42:075413

Kolitsch U, Holtstam D (2004) Crystal chemistry of $REEXO_4$ compounds (X= P, As, V). II. review of $REEXO_4$ compounds and their stability fields. Eur J Mineral 16:117–126

Kolitsch U, Holtstam D, Gatedal K (2004) Crystal chemistry of $REEXO_4$ compounds (X= P, As, V). I. paragenesis and crystal structure of phosphatian gasparite-(Ce) from the Kesebol Mn-Fe-Cu deposit, Västra Götaland, Sweden. Eur J Mineral 16:111–116

Lacomba-Perales R, Errandonea D, Meng Y, Bettinelli M (2010) High-pressure stability and compressibility of $APO_4$ (A= La, Nd, Eu, Gd, Er, and Y) orthophosphates: an x-ray diffraction study using synchrotron radiation. Phys Rev B 81:064113

Li H, Zhang S, Zhou S, Cao X (2009) Bonding characteristics, thermal expansibility, and compressibility of $RXO_4$ (R= Rare Earths, X= P, As) within monazite and zircon structures. Inorg Chem 48:4542–4548

Mancini S (2000) Le mineralizzazioni a manganese delle Alpi Apuane. Thesis dissertation, University of Pisa

Mao HK, Xu JA, Bell PM (1986) Calibration of the ruby pressure gauge to 800 kbar under quasi-hydrostatic conditions. J Geophys Res Solid Earth 91:4673–4676

Merlini M, Hanfland M (2013) Single-crystal diffraction at megabar conditions by synchrotron radiation. High Pressure Res 33:511–522

Metzger SJ, Ledderboge F, Heymann G, Huppertz H, Schleid T (2016) High-pressure investigations of lanthanoid oxoarsenates: I. Single crystals of scheelite-type $Ln[AsO_4]$ phases with Ln=La–Nd from monazite-type precursors. Z Naturforsch B 71:439–445

Mills SJ, Kartashov PM, Kampf AR, Raudsepp M (2010) Arsenoflorencite-(La), a new mineral from the Komi Republic, Russian

Federation: description and crystal structure. Eur J Mineral 22:613–621
Momma K, Izumi F (2011) VESTA 3 for three-dimensional visualization of crystal, volumetric and morphology data. J Appl Crystallogr 44:1272–1276
Mooney RC (1948) Crystal structures of a series of rare earth phosphates. J Chem Phys 16:1003–1003
Muller O, Roy R (1974) Crystal chemistry of non-metallic materials, The major ternary structural families, vol 4. Springer-Verlag, New York/Heidelberg/Berlin
Mullica DF, Milligan WO, Grossie DA, Beall GW, Boatner LA (1984) Ninefold coordination $LaPO_4$: pentagonal interpenetrating tetrahedral polyhedron. Inorg Chim Acta 95:231–236
Muñoz A, Rodríguez-Hernández P (2018) High-pressure elastic, vibrational and structural study of monazite-type $GdPO_4$ from ab initio simulations. Cryst 8:209
Ni Y, Hughes JM, Mariano AN (1995) Crystal chemistry of the monazite and xenotime structures. Am Min 80:21–26
Ondrejka M, Uher P, Pršek J, Ozdín D (2007) Arsenian monazite-(Ce) and xenotime-(Y), REE arsenates and carbonates from the Tisovec-Rejkovo rhyolite, Western Carpathians, Slovakia: composition and substitutions in the (REE, Y)$X_O$4 system (X= P, As, Si, Nb, S). Lithos 95:116–129
OriginLab Corporation (2019) OriginPro, Northampton, MA, USA
Pagliaro F, Lotti P, Guastoni A, Rotiroti N, Battiston T, Gatta GD (2022) Crystal chemistry and miscibility of chernovite-(Y), xenotime-(Y), gasparite-(Ce) and monazite-(Ce) from Mt. Cervandone (Western Alps, Italy). Min Mag 86:1–18
Petříček V, Dušek M, Palatinus L (2014) Crystallographic computing system JANA2006: general features. Z Kristallogr 229:345–352
Rice CE, Robinson WR (1976) Lanthanum orthophosphate. Acta Crystallogr B 32:2232–2233
Rigaku Oxford Diffraction (2019) CrysAlisPro Software system, version 1.171.40.67a. Rigaku Corporation, Wroclaw
Ruiz-Fuertes J, Hirsch A, Friedrich A, Winkler B, Bayarjargal L, Morgenroth W, Peters L, Roth G, Milman V (2016) High-pressure phase of $LaPO_4$ studied by x-ray diffraction and second harmonic generation. Phys Rev B 94:134109
Ushakov SV, Helean KB, Navrotsky A, Boatner LA (2001) Thermochemistry of rare-earth orthophosphates. J Mater Res 16:2623–2633
Vereshchagin OS, Britvin SN, Perova EN, Brusnitsyn AI, Polekhovsky YS, Shilovskikh VV, Bocharov VN, van der Burgt A, Cuchet S, Meisser N (2019) Gasparite-(La), La($AsO_4$), a new mineral from Mn ores of the Ushkatyn-III deposit, Central Kazakhstan, and metamorphic rocks of the Wanni glacier, Switzerland. Am Min 104:1469–1480